Detection, Synchronization, and Doppler Scale Estimation with Multicarrier Waveforms in Underwater Acoustic Communication

Sean Mason, *Student Member, IEEE,* Christian R. Berger, *Student Member, IEEE,*
Shengli Zhou, *Member, IEEE*, and Peter Willett, *Fellow, IEEE*

Index Terms

Underwater acoustic communication, multicarrier, OFDM, synchronization,
detection, Doppler scale estimation

This work is supported by the ONR YIP grant N00014-07-1-0805, the NSF grant ECS 0725562, the NSF grant CNS 0721834, and the ONR grant N00014-07-1-0055.

S. Mason, C. R. Berger, S. Zhou and P. Willett are with the Department of Electrical and Computer Engineering, University of Connecticut, 371 Fairfield Way U-2157, Storrs, Connecticut 06269, USA (email: {seanm, crberger, shengli, willett}@engr.uconn.edu).

S. Zhou is the contact author. Phone: 860-486-4593, Email: shengli@engr.uconn.edu

Abstract

In this paper, we propose a novel method for detection, synchronization and Doppler scale estimation for underwater acoustic communication using orthogonal frequency division multiplex (OFDM) waveforms. This new method involves transmitting two identical OFDM symbols together with a cyclic prefix, while the receiver uses a bank of parallel self-correlators. Each correlator is matched to a different Doppler scaling factor with respect to the waveform dilation or compression. We characterize the receiver operating characteristic in terms of probability of false alarm and probability of detection. We also analyze the impact of Doppler scale estimation accuracy on the data transmission performance. These analytical results provide guidelines for the selection of the detection threshold and Doppler scale resolution. In addition to computer-based simulations, we have tested the proposed method with real data from an experiment at Buzzards Bay, MA, Dec. 15, 2006. Using only one preamble, the proposed method achieves similar performance on the Doppler scale estimation and the bit error rate as an existing method that uses two linearly-frequency-modulated (LFM) waveforms, one as a preamble and the other as a postamble, around each data burst transmission. Compared with the LFM based method, the proposed method works with a constant detection threshold independent of the noise level and is suited to handle the presence of dense multipath channels. More importantly, the proposed approach avoids the need of buffering the whole data packet before data demodulation, which enables online receiver operation for multicarrier underwater acoustic communications.

I. INTRODUCTION

Various data transmission schemes are being actively pursued for underwater acoustic (UWA) communications, including multicarrier modulation in the form of orthogonal frequency division multiplexing (OFDM) [1], [2], [3], [4], [5], single carrier transmission with time-domain sparse-channel equalization [6] or frequency-domain equalization [7], and multi-input multi-output (MIMO) techniques combined with single carrier [8], [9] or multicarrier [10] transmissions. These transmission schemes are often examined via *offline* data processing based on recorded experimental data. Towards the development of an *online* underwater acoustic receiver, detection and synchronization are important, yet often overlooked tasks.

Typically, synchronization entails a known preamble, which is easily detected by the receiver, being transmitted prior to the data. Existing preambles used in underwater telemetry are almost exclusively based on linearly frequency modulated (LFM) signals, also known as Chirp signals [11]. This is due to the fact that LFM signals have a desirable ambiguity function in both time and frequency, which matches well to the underwater channel, which is characterized by its large Doppler spread. However, the receiver algorithms are usually matched-filter based, which try to synchronize a known template to the signal coming from one strong path, while suppressing other interfering paths. This approach suffers from the following two deficiencies: first, the noise level at the receiver has to be constantly estimated to achieve a constant false alarm rate (CFAR), usually accomplished using order statistics; second, its performance will degrade in the presence of dense and unknown multipath channels.

Due to the slow propagation speed of acoustic waves, the compression or dilation effect on the time domain waveform needs to be considered explicitly. Once a Doppler scale estimate is obtained, a resampling procedure is usually applied before data demodulation [12]. One method to estimate the Doppler scale is to use an LFM preamble and an LFM postamble around each data burst [12], so that the receiver can estimate the change of the

waveform duration. However, with this method, the whole data burst has to be buffered before data demodulation, which prevents real time receiver processing.

In this paper, we propose the use of multicarrier waveforms as preamble for underwater acoustic communications. A preamble that consists of two identical OFDM symbols preceded by a cyclic prefix (CP) is used. This training pattern has been studied extensively in wireless OFDM systems for radio channels, see e.g., [13], [14], and has been included as part of the training preamble in the IEEE 802.11a/g standards [15]. The receiver effectively correlates the received signal with a delayed version of itself, since, thanks to the CP structure, the repetition pattern persists even in the presence of unknown multipath channels [13]. However, the synchronization algorithms that work in wireless radio channels will not perform well in dynamic underwater acoustic channels due to the large waveform expansion or compression, which changes the repetition period to some unknown value.

We develop a novel method that utilizes multicarrier waveforms for detection, synchronization and Doppler scale estimation. We use a bank of parallel branches, with each branch using a self-correlator matched to a different repetition period. Detection of a data transmission burst is declared when any of the branches leads to a correlation metric larger than a threshold value. The branch with the largest metric also yields the Doppler scale estimate and coarse synchronization point. We characterize the receiver operating characteristic (ROC) by developing an analytical expression for the probability of false alarm and a Gaussian approximation for the probability of detection. We also analyze the impact of Doppler scale estimation accuracy on the data demodulation performance. These analytical results provide guidelines for selecting the detection threshold and Doppler scale resolution. Compared with the LFM-preamble based approach, the proposed method has the following advantages: (1) the detection threshold is between 0 and 1, and doesn't depend on the channel or operating SNR; (2) it has a very good detection performance, which is based on the signal energy from *all* paths rather than only a single path; (3) it leads to accurate Doppler scale estimation; (4) after coarse timing and resampling, it allows the use of fine timing algorithms developed for radio channels, such as [16], [17].

In addition to computer-based simulations, we have tested the proposed method with real data from an experiment at Buzzards Bay, MA, Dec. 15, 2006. Using only one preamble, the proposed method achieves similar performance on the Doppler scale estimation accuracy and the bit error rate as those methods presented in [5], which are based on the LFM preamble and postamble. However, the proposed method avoids the need of using a postamble and buffering the whole data packet before demodulation. This enables online receiver operation for multicarrier underwater acoustic communications.

The rest of this paper is as follows. The system model is described in Section II, and the proposed receiver algorithm is presented in Section III. Detection performance is determined in Section IV, and analysis of the impact of Doppler scale mismatch on the data demodulation performance is investigated in Section V. Section VI contains numerical results, both from simulation and from real data. Section VII contains the conclusion.

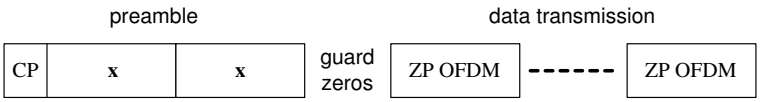

Fig. 1. A preamble, consisting of two identical OFDM symbols and a cyclic prefix (CP), precedes the data transmission which uses zero padding.

II. System Model

To avoid power consumption in the guard interval between OFDM symbols, zero-padded (ZP) OFDM is preferred for data transmission [3], [4], [5]. For synchronization purposes, the preamble consists of two identical OFDM symbols together with a cyclic prefix. The overall transmission structure is shown in Fig. 1. The OFDM parameters can be selected independently for the preamble and the data transmissions.

Suppose that K_0 subcarriers have been used in the preamble, and one OFDM symbol is of duration T_0. The subcarrier spacing is then $1/T_0$ and the bandwidth is $B = K_0/T_0$. Let f_c denote the carrier frequency, and $f_k = f_c + k/T_0$ denote the frequency for the kth subcarrier in passband, where $k \in \mathcal{S} = \{-K_0/2, \ldots, K_0/2 - 1\}$. Let $T_{\rm cp}$ denote the length of the CP, and define a rectangular window of length $T_{\rm cp} + 2T_0$ as

$$q(t) = \begin{cases} 1 & t \in [-T_{\rm cp}, 2T_0], \\ 0 & \text{otherwise.} \end{cases} \tag{1}$$

The preamble in baseband can be written as

$$x(t) = \sum_{k \in \mathcal{S}} s[k] e^{j2\pi \frac{k}{T_0} t} q(t) \tag{2}$$

and the corresponding passband signal is

$$\tilde{x}(t) = \text{Re}\left\{ e^{j2\pi f_c t} \sum_{k \in \mathcal{S}} s[k] e^{j2\pi \frac{k}{T_0} t} q(t) \right\} = \text{Re}\left\{ \sum_{k \in \mathcal{S}} s[k] e^{j2\pi f_k t} q(t) \right\}, \tag{3}$$

where $s[k]$ is the transmitted symbol on the kth subcarrier.

The channel impulse response for a time-varying multipath underwater acoustic channel can be described by

$$c(\tau, t) = \sum_p A_p(t) \delta\left(\tau - \tau_p(t)\right), \tag{4}$$

where $A_p(t)$ is the path amplitude and $\tau_p(t)$ is the time-varying path delay. As in [5], [18], we assume that all paths have a similar Doppler rate,

$$\tau_p(t) \approx \tau_p - at, \tag{5}$$

and that the path gains A_p, the transmission delay τ_p and the Doppler rate a are constant over the duration of the preamble. When these assumptions do not hold true, part of the useful signal is treated as additive noise, which increases the overall noise variance, as pointed out in [5], [18].

When the passband signal in (3) goes through the channel described in (4) and (5), we receive:

$$\tilde{y}(t) = \text{Re}\left\{\sum_{k\in\mathcal{S}} s[k]e^{j2\pi f_k(1+a)t}\sum_p A_p q\big((1+a)t-\tau_p\big)e^{-j2\pi f_k\tau_p}\right\} + \tilde{n}(t), \tag{6}$$

where $\tilde{n}(t)$ is the additive noise. Define $\tau_{\max} = \max_p \tau_p$, which is usually less than the CP length T_{cp}. Using the definition of $q(t)$ in (1), we obtain

$$\tilde{y}(t) = \text{Re}\left\{\sum_{k\in\mathcal{S}} H_k s[k]e^{j2\pi f_k(1+a)t}\right\} + \tilde{n}(t), \quad t\in\mathcal{T}_{\text{cyclic}} = \left[-\frac{T_{\text{cp}}-\tau_{\max}}{1+a}, \frac{2T_0}{1+a}\right], \tag{7}$$

where we define the channel transfer function

$$C(f) = \sum_p A_p e^{-j2\pi f\tau_p} \tag{8}$$

and the frequency response on the kth subcarrier as

$$H_k = C(f_k). \tag{9}$$

Converting the passband signal $\tilde{y}(t)$ to baseband, such that $\tilde{y}(t) = \text{Re}\left\{y(t)e^{j2\pi f_c t}\right\}$, we have:

$$y(t) = \sum_{k\in\mathcal{S}} H_k s[k]e^{j2\pi\left(\frac{k}{T_0}+af_k\right)t} + n(t) \tag{10}$$

$$= e^{j2\pi af_c t}\sum_{k\in\mathcal{S}} H_k s[k]e^{j2\pi\frac{k}{T_0}(1+a)t} + n(t), \quad t\in\mathcal{T}_{\text{cyclic}}, \tag{11}$$

where $n(t)$ is the noise at baseband.

As expected for CP-OFDM, we observe a cyclic convolution between the signal and the channel in the specified interval, where each subcarrier is only multiplied by the corresponding frequency response. Due to the wideband nature of the underwater channel, the frequency of each subcarrier at baseband has been shifted differently by an amount of $af_k = af_c + ak/T_0$.

III. The Proposed Algorithm

The transmitter sends a baseband waveform embedding a repetition pattern as

$$x(t) = x(t+T_0), \quad -T_{\text{cp}} \le t \le T_0. \tag{12}$$

Such a repetition pattern persists in the received signal $y(t)$ even after time-varying multipath propagation as

$$y(t) = e^{-j2\pi\frac{a}{1+a}f_c T_0} y\left(t+\frac{T_0}{1+a}\right), \quad -\frac{T_{\text{cp}}-\tau_{\max}}{1+a} \le t \le \frac{T_0}{1+a}, \tag{13}$$

as can be verified from (11). However, the receiver knows neither the *period* nor the *waveform* due to the unknown multipath channel. The problem is then to detect a pattern like (13) from the incoming signal, and infer the repetition period to find the Doppler scale.

Our proposed approach is to use a bank of self-correlators, see Fig 2, with each one matched to a different periodicity. Detection, synchronization, and Doppler scale estimation are accomplished based on the correlation metrics from the bank of self-correlators.

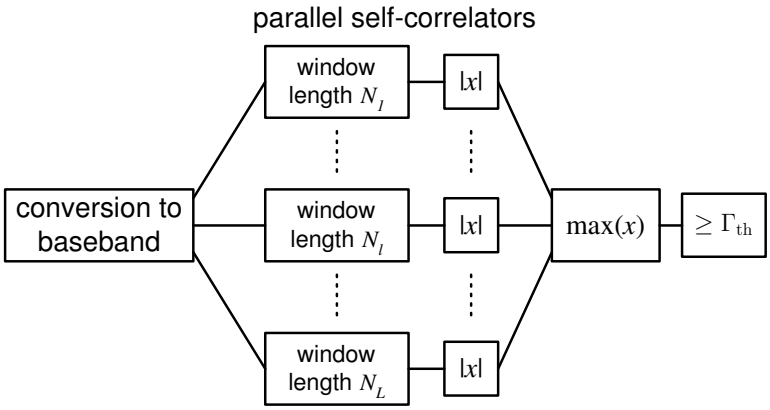

Fig. 2. To account for the time compression/dilation, multiple parallel branches are used, each tuned to a certain period N_l.

We now present the proposed receiver processing, based on the sampled baseband signal. The baseband signal is usually oversampled at a multiple of the system bandwidth $t_s = 1/(\lambda B)$:

$$y[n] = y(t)|_{t=nt_s}. \tag{14}$$

The receiver processing includes the following steps:

1) Each of the L branches calculates a correlation metric with one candidate value of the window size N_l, for each delay d,

$$M(N_l, d) = \frac{\sum_{i=d}^{d+N_l-1} y^*[i]\, y[i+N_l]}{\sqrt{\sum_{i=d}^{d+N_l-1} |y[i]|^2 \cdot \sum_{i=d}^{d+N_l-1} |y[i+N_l]|^2}}, \quad l = 1, \ldots L. \tag{15}$$

The window size N_l shall be close to λK_0, which is the number of samples of one OFDM symbol when no Doppler scaling occurs.

2) A detection is declared if the correlation metric of any branch exceeds a preset threshold $\Gamma_{\rm th}$:

$$H_1 \quad \text{if:} \quad \max_l |M(N_l, d)| > \Gamma_{\rm th} \tag{16}$$

Since the norm of the metric in (15) is between 0 and 1, the threshold $\Gamma_{\rm th}$ takes a value from [0,1].

3) The branch with the largest correlation metric is viewed as having the best match on the repetition length. Since Doppler scaling changes the period T_0 to $T_0/(1+a)$, the Doppler scale factor can be estimated as

$$\hat{a} = \frac{\lambda K_0 - \hat{N}}{\hat{N}}, \quad \text{where } \hat{N} = \arg\max_{\{N_l\}} |M(N_l, d)| \tag{17}$$

The speed estimate follows as

$$\hat{v} = c\hat{a}, \tag{18}$$

where c is the speed of sound in water. Additional processing can be used to refine the Doppler scale estimate, as will be shown later on in Section VI.

4) Synchronization is performed on the branch that yields the maximum correlation metric. After the maximum is determined, the start of transmission can be selected as suggested in [13]; starting from the peak the 80%

"shoulders" are found (first sample of this correlator branch before and after the peak that is less than 80% of the peak) and the middle is chosen as synchronization point. This is beneficial, since due to the CP structure the correlation metric has a plateau around the peak [13].

Remark 1: Since the window size N_l is an integer, the minimum step size on the Doppler scale is $1/(\lambda K_0)$. To improve the Doppler scale resolution, the receiver operates on the oversampled baseband signal. The oversampling factor depends on the needed Doppler scale resolution and the parameter K_0.

Remark 2: With the estimated Doppler scale $\hat{a}$, the receiver can resample the preamble. This way, the "wideband" channel effect of frequency-dependent Doppler shifts can be reduced to the "narrowband" channel effect of frequency-independent Doppler shifts [5]. The fine-timing algorithms developed for narrowband radio channels, such as those in [16], [17] can be applied on the resampled preamble. This way, the "first" path can be synchronized [17], instead of the "strongest" path in case of the LFM based method.

So far, we have described the general procedure of the proposed detection, synchronization, and Doppler scale estimation algorithm, while some parameters are left to be specified. Important questions include:

- *How to set the detection threshold?*
- *How many parallel branches are needed? What is the desired Doppler scale resolution?*

We next address these questions by analyzing the detection performance in Section IV, and the data demodulation performance under Doppler scale mismatch in Section V.

IV. Receiver Operating Characteristics

The output of each correlator is a random variable due to the additive noise. The probabilities of false alarm P_{fa} and detection P_d are the probabilities of the correlator output exceeding a threshold $\Gamma_{\rm th}$ under the "no signal" and "signal" hypotheses, respectively. We now analyze the false alarm and detection probabilities of a single branch, as a function of the threshold $\Gamma_{\rm th}$ and the Doppler scale a. This will give us an understanding of the necessary Doppler scale spacing in the parallel self-correlator structure for detection purposes. Due to over-sampling, the summations in the metric given in (15) of the lth branch can be well approximated with continuous time integrals:

$$M\left(\hat{T},t\right)=\frac{\int_t^{t+\hat{T}} y(\tau)^* y(\tau+\hat{T})\,d\tau}{\sqrt{\int_t^{t+\hat{T}}|y(\tau)|^2\,d\tau\cdot\int_t^{t+\hat{T}}\left|y(\tau+\hat{T})\right|^2\,d\tau}}, \tag{19}$$

where

$$\hat{T}=N_l\cdot t_s=\frac{T_0}{1+\hat{a}},\quad t=d\cdot t_s. \tag{20}$$

A. Probability of False Alarm

When no signal is present, $y(t) = n(t)$. Since $B\hat{T} \approx K_0$, we can find a set of orthonormal basis functions $\{f_i(t)\}_{i=0}^{K_0-1}$, such that

$$n(\tau) = \sum_{i=0}^{K_0-1} n_{t,i} f_i(\tau), \quad \tau \in [t, t+\hat{T}] \tag{21}$$

$$n(\tau+\hat{T}) = \sum_{i=0}^{K_0-1} n_{t+\hat{T},i} f_i(\tau), \quad \tau \in [t, t+\hat{T}]. \tag{22}$$

Assume that $n(t)$ is a Gaussian noise process, then $n_{t,i}$ and $n_{t+\hat{T},i}$ are independent and identically distributed Gaussian random variables. Define[1] $\mathbf{n}_t = [n_{t,0}, \ldots, n_{t,K_0-1}]^T$ and $\mathbf{n}_{t+\hat{T}} = [n_{t+\hat{T},0}, \ldots, n_{t+\hat{T},K_0-1}]^T$, and their normalized versions $\tilde{\mathbf{n}}_t = \mathbf{n}_t/\|\mathbf{n}_t\|$ and $\tilde{\mathbf{n}}_{t+\hat{T}} = \mathbf{n}_{t+\hat{T}}/\|\mathbf{n}_{t+\hat{T}}\|$. The correlator output (19) can be simplified to the inner product between two unit length vectors as

$$M\left(\hat{T}, t\right) = \tilde{\mathbf{n}}_t^{\mathcal{H}} \tilde{\mathbf{n}}_{t+\hat{T}}. \tag{23}$$

Finding the probability of false alarm can now be linked to the Grassmannian line packing problem in [19]. Specifically, $\tilde{\mathbf{n}}_t$ can be viewed as coordinates of a point on the surface of a hypersphere with unit radius, centered around the origin. This point dictates a straight line in a complex space $\mathcal{C}^{K_0}$ that passes through the origin. The two lines generated by $\tilde{\mathbf{n}}_t$ and $\tilde{\mathbf{n}}_{t+\hat{T}}$ have a distance defined as:

$$d(\tilde{\mathbf{n}}_t, \tilde{\mathbf{n}}_{t+\hat{T}}) := \sin(\theta_t) = \sqrt{1 - |\tilde{\mathbf{n}}_t^{\mathcal{H}} \tilde{\mathbf{n}}_{t+\hat{T}}|^2}, \tag{24}$$

where θ_t denotes the angle between these two lines. The distance $d(\tilde{\mathbf{n}}_t, \tilde{\mathbf{n}}_{t+\hat{T}})$ is known as "chordal distance" [19]. Since $n(t)$ is additive white and Gaussian, $\tilde{\mathbf{n}}_t$ and $\tilde{\mathbf{n}}_{t+\hat{T}}$ are uniformly distributed on the surface of the hypersphere. Without loss of generality, we can assume that $\tilde{\mathbf{n}}_{t+\hat{T}}$ is fixed a priori and $\tilde{\mathbf{n}}_t$ is uniformly distributed, to evaluate the distribution of the chordal distance. Based on [20, eq. (34)] (which was derived based on the geometrical framework in [21]), we infer

$$\Pr\left\{d^2(\tilde{\mathbf{n}}_t, \tilde{\mathbf{n}}_{t+\hat{T}}) < z\right\} = z^{K_0-1}, \quad 0 < z < 1. \tag{25}$$

Hence, the probability of false alarm is

$$P_{fa} = \Pr\left\{|M(\hat{T}, t)| > \Gamma_{\text{th}}\right\} \tag{26a}$$

$$= \Pr\left\{d^2(\tilde{\mathbf{n}}_t, \tilde{\mathbf{n}}_{t+\hat{T}}) < 1 - \Gamma_{\text{th}}^2\right\} \tag{26b}$$

$$= (1 - \Gamma_{\text{th}}^2)^{K_0-1}. \tag{26c}$$

Note that P_{fa} does not depend on the power of the additive noise. Once the threshold Γ_{th} is chosen, a constant false alarm rate (CFAR) is achieved independent of the noise level.

[1]Bold upper case and lower case letters denote matrices and column vectors, respectively; $(\cdot)^T$, $(\cdot)^*$, and $(\cdot)^{\mathcal{H}}$ denote transpose, conjugate, and Hermitian transpose, respectively. $|\cdot|$ and $\|\cdot\|$ stand for for the absolute value of a complex number and the norm of a vector, respectively.

B. Probability of Detection

Assume that the signal is present, we rewrite (11) as

$$y(t) = x_c(t) + n(t), \tag{27}$$

where the signal is

$$x_c(t) = e^{j2\pi a f_c t} \sum_{k\in\mathcal{S}} H_k s[k] e^{j2\pi \frac{k}{T_0}(1+a)t}, \quad t \in \mathcal{T}_{\text{cyclic}}. \tag{28}$$

Treating the signal as deterministic unknown, we define the autocorrelation function of $x_c(t)$ as

$$\phi_{xx}(T, \Delta T) = \frac{1}{T}\int_t^{t+T} x_c(\tau) x_c(\tau + \Delta T) d\tau. \tag{29}$$

The noise is viewed as wide sense stationary, and we define its autocorrelation function as $\phi_{nn}(\tau)$. Assuming that the integration is done in a proper window where $x_c(t)$ is well defined as in (28), we can easily obtain:

$$E\Big\{\int_t^{t+\hat{T}} y(\tau)^* y(\tau+\hat{T})\, d\tau\Big\} = \hat{T}\phi_{xx}(\hat{T},\hat{T}), \quad t \in \mathcal{T}_{\text{plateau}} := \left[-\frac{T_{\text{cp}} - \tau_{\max}}{1+a}, \frac{2T_0(\hat{a}-a)}{(1+a)(1+\hat{a})}\right] \tag{30}$$

$$E\Big\{\int_t^{t+\hat{T}} |y(\tau)|^2 d\tau\Big\} = E\Big\{\int_t^{t+\hat{T}} |y(\tau+\hat{T})|^2 d\tau\Big\} = \hat{T}[\phi_{xx}(\hat{T},0) + \phi_{nn}(0)], \quad t \in \mathcal{T}_{\text{plateau}}. \tag{31}$$

In [13], the absolute value of the correlation metric has been approximated as a Gaussian random variable to derive some approximate results. We would like to follow the same principle here. To this end, we propose to approximate the mean of the correlator output as:

$$\mathrm{E}\left\{\left|M\left(\hat{T}, t\right)\right|\right\} \approx \frac{\hat{T}|\phi_{xx}(\hat{T},\hat{T})|}{\hat{T}\phi_{xx}(\hat{T},0) + \hat{T}\phi_{nn}(0)} = \frac{\alpha\gamma}{\gamma+1}, \quad t \in \mathcal{T}_{\text{plateau}}, \tag{32}$$

where $\gamma = \phi_{xx}(\hat{T},0)/\phi_{nn}(0)$ is the signal-to-noise-ratio (SNR) at the receiver, and α is the correlation coefficient

$$\alpha = \frac{|\phi_{xx}(\hat{T},\hat{T})|}{\phi_{xx}(\hat{T},0)}. \tag{33}$$

The variance can be approximated as

$$\mathrm{Var}\left\{\left|M\left(\hat{T}, t\right)\right|\right\} \approx \frac{2\gamma^3 + 5\gamma^2 + 3\gamma + 1}{2K_0(\gamma+1)^4}, \quad t \in \mathcal{T}_{\text{plateau}}. \tag{34}$$

The variance in (34) was derived in the radio channel case without Doppler scaling where $|\alpha| = 1$. We argue that it can still be used in the case with Doppler scaling, since the variation of the correlation output is mainly due to additive noise.

We now specify the correlation coefficient α. Based on (28), we have for $t \in \mathcal{T}_{\text{plateau}}$

$$\phi_{xx}(\hat{T},\hat{T}) = \frac{1}{\hat{T}}\int_t^{t+\hat{T}} \left[x_c^*(\tau) x_c(\tau+\hat{T})\right] d\tau \tag{35a}$$

$$= e^{-j2\pi a f_c \hat{T}} \sum_{k\in\mathcal{S}}\sum_{l\in\mathcal{S}} H_k s[k] H_l^* s[l]^* \frac{1}{\hat{T}}\int_t^{t+\hat{T}} \exp\left(j2\pi(1+a)\left[\frac{k}{T_0}\tau - \frac{l}{T_0}(\tau+\hat{T})\right]\right) d\tau, \tag{35b}$$

which lead to

$$|\phi_{xx}(\hat{T},\hat{T})| = \Big|\sum_{k\in\mathcal{S}}\sum_{l\in\mathcal{S}} H_k s[k] H_l^* s[l]^* e^{-j2\pi(1+\epsilon)l} e^{j\pi(1+\epsilon)(k-l)} \operatorname{sinc}\left[(1+\epsilon)(k-l)\right]\Big|, \tag{36}$$

where $\text{sinc}(x) = \sin(\pi x)/(\pi x)$ and $(1+\epsilon) = (1+a)/(1+\hat{a})$. Therefore, $\epsilon \approx a - \hat{a}$. Assume that ϵ is tiny, we approximate $\text{sinc}[(1+\epsilon)(k-l)] \approx \delta[k-l]$. For constant amplitude modulation $|s[i]|^2 = \sigma_s^2$, we have

$$|\phi_{xx}(\hat{T}, \hat{T})| \approx \sigma_s^2 \left| \sum_{k \in \mathcal{S}} |H_k|^2 e^{-j2\pi k(a-\hat{a})} \right|. \tag{37}$$

Similar approximation can be done for $\phi_{xx}(\hat{T}, 0)$. We thus have

$$\alpha \approx \frac{\left| \sum_{k \in \mathcal{S}} |H_k|^2 e^{-j2\pi k(a-\hat{a})} \right|}{\sum_{k \in \mathcal{S}} |H_k|^2}. \tag{38}$$

In summary, with α approximated in (38), the mean μ_α approximated in (32), and the variance σ_α approximated in (34), an approximate expression for the probability of detection in $\mathcal{T}_{\text{plateau}}$ is

$$P_d = \Pr\left\{ \left| M\left(\hat{T}, t\right) \right| \geq \Gamma_{\text{th}} \right\} \approx Q\left(\frac{\Gamma_{\text{th}} - \mu_\alpha}{\sigma_\alpha} \right), \tag{39}$$

where $Q(x) = (1/\sqrt{2\pi}) \int_x^\infty e^{-t^2/2} dt$.

C. Numerical Validation

To confirm the theoretical analysis, we use numerical simulation using the following steps:

1) Generate the baseband signal via (11) and sample it as in (14).
2) Compare the statistics of the correlator output at signal start $t = 0$ on a branch with $N_l = \lambda K_0$.

For the non-dispersive channel with a single path, the mean of the correlator can be simplified to

$$\text{E}\left\{ \left| M\left(\hat{T}, 0\right) \right| \right\} = \frac{\alpha\gamma}{\gamma+1} = |\text{sinc}\left[K(a-\hat{a})\right]| \frac{\gamma}{\gamma+1}. \tag{40}$$

The simulation results for the non-dispersive channel are shown in Fig. 3(a); we observe that the loss of correlation due to the unknown speed is modelled well by the sinc function, while the approximation of the standard deviation is fairly exact for the low SNR case but only of the right magnitude for the high SNR case.

For dispersive channels we average over different channel realizations, where we choose an exponentially decaying channel profile that loses about 20 dB within 10 ms. For each channel realization, we evaluate the mean and variance of the Gaussian approximation, then average these by approximating them via a single Gaussian distribution with matched moments. Since this is basically a Gaussian mixture distribution, the resulting mean is the average mean, while the variance is increased: it consists of the average variance and the additional "spread" of the means.

The results are in Fig. 3(b); we see an identical behavior for $K(a-\hat{a}) \ll 1$ (inside the main lobe of the sinc function). This is because for $\epsilon \approx a - \hat{a} = 0$, α is fixed as unity (c.f. (38)), while for $\epsilon \neq 0$, α is a random variable depending on the specific channel realization. Accordingly the additional variation in α leads to an increased variance for larger ϵ and the sinc shape is distorted depending on the channel statistics. Still, for a small speed mismatch the behavior can be well approximated by the non-dispersive channel.

To assess the effect of Doppler scale mismatch, i.e., unknown speed, on the detection performance, we plot the receiver operating characteristic (ROC) in Fig. 4. The exact probability of false alarm (26c) is plotted against the Gaussian approximation as well as Monte-Carlo simulation results for both AWGN and dispersive channels. For

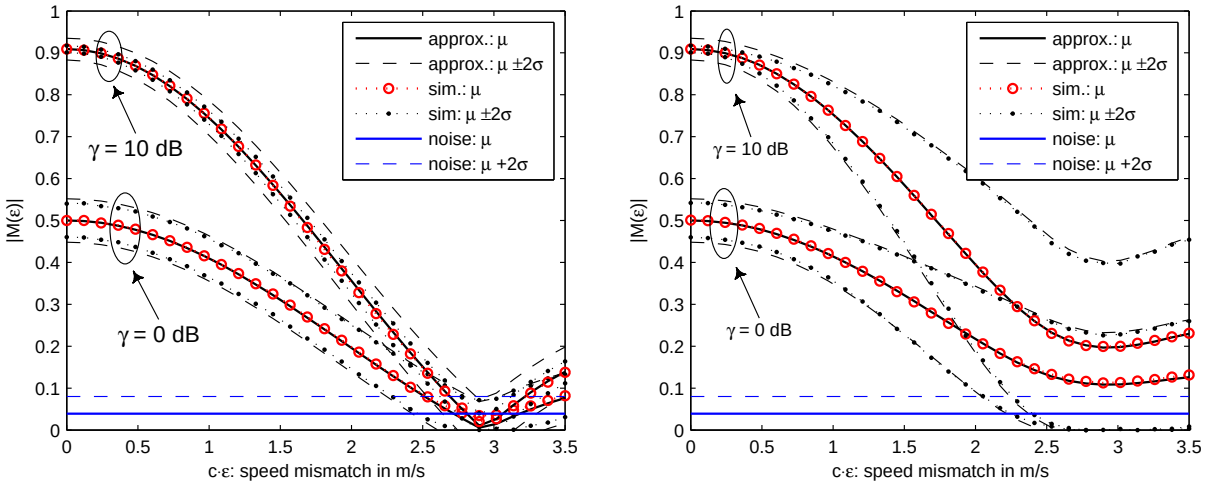

(a) non-dispersive (b) dispersive

Fig. 3. Statistics of the correlator output, including the mean μ and standard deviation σ as a function of the unknown speed for two different levels of SNR γ; (a) non-dispersive channel with a single path, (b) dispersive channel with an exponential decay profile.

the non-dispersive case we see that the simulation results match the Gaussian approximation reasonably for the chosen speeds and SNR. Comparing to Fig. 3, the detection performance is superb as long as the mean, μ_α, of the correlator output under the signal hypothesis and the mean under the noise hypothesis are separated by more than six times the standard deviation, σ_α.

In case of the dispersive channel, we had seen in Fig. 3 that the mean μ_α of the correlator was always higher for large Doppler scales, but at the cost of an increased variance. This results in the ROC's having less steep slopes, intersecting the curves for the AWGN channel – accordingly performing better for detection probabilities around one half, but worse towards one (that are the regions of interest). This detrimental effect is negligible when the Doppler scale mismatch is less than, e.g., $c(a - \hat{a}) \approx 1.5$ m/s, which are also the regions of generally good performance. Therefore for a limited Doppler scale mismatch, the detection performance is not changed much by the dispersive nature of the channel.

V. Impact of Doppler Scale Estimation Accuracy

In this section, we analyze the performance degradation on data transmission due to the Doppler scale mismatch. This will help to specify the needed Doppler scale resolution from a data communication perspective.

For data transmission, we use ZP-OFDM. Since block by block processing is used, let us focus on one ZP-OFDM block. Let T denote the OFDM symbol duration and T_g the guard interval. The total OFDM block duration is $T' = T + T_g$ and the subcarrier spacing is $1/T$. The kth subcarrier is at frequency

$$f_k = f_c + k/T, \quad k = -K/2, \ldots, K/2 - 1, \tag{41}$$

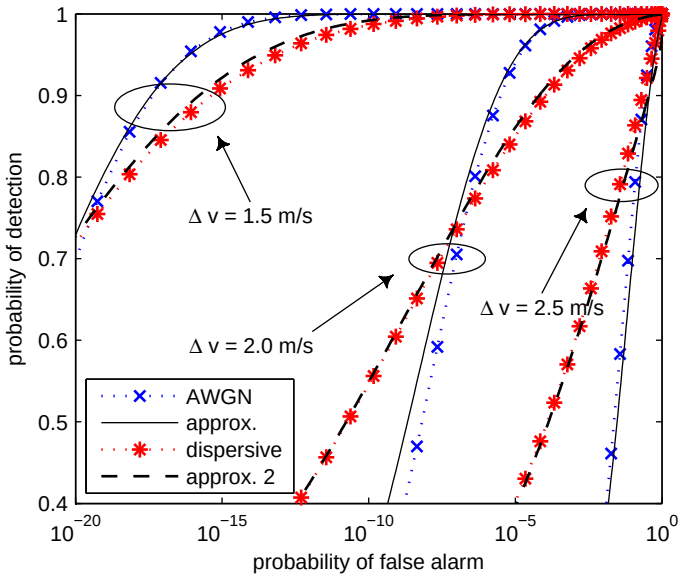

Fig. 4. Receiver operating characteristic (ROC) of the detection scheme for $K_0 = 512$ OFDM carriers, $\gamma = 0$ dB and varying speeds; plotted are the Gaussian approximation of the probability of detection and simulated probability of detection for different channels against the exact analytic probability of false alarm.

where f_c is the carrier frequency and K subcarriers are used so that the bandwidth is $B = K/T$. Let $s[k]$ denote the information symbol to be transmitted on the kth subcarrier. The non-overlapping sets of active subcarriers $\mathcal{S}_A$ and null subcarriers $\mathcal{S}_N$ satisfy $\mathcal{S}_A \cup \mathcal{S}_N = \{-K/2, \ldots, K/2-1\}$; the null subcarriers are used to facilitate Doppler compensation at the receiver [5], [18]. The transmitted signal in passband is then given by

$$x(t) = \mathrm{Re}\left\{ \left[\sum_{k \in \mathcal{S}_\mathrm{A}} s[k] e^{j2\pi \frac{k}{T} t} g(t) \right] e^{j2\pi f_c t} \right\}, \quad t \in [0, T + T_g], \tag{42}$$

where $g(t)$ describes the zero-padding operation, i.e., $g(t) = 1, t \in [0, T]$ and $g(t) = 0$ otherwise. Due to the adopted channel model, the received passband signal is

$$\tilde{y}(t) = \mathrm{Re}\left\{ \sum_p A_p \left[\sum_{k \in \mathcal{S}_A} s[k] e^{j2\pi \frac{k}{T}(t+at-\tau_p)} g(t + at - \tau_p) \right] e^{j2\pi f_c (t+at-\tau_p)} \right\} + \tilde{n}(t), \tag{43}$$

where $\tilde{n}(t)$ is the additive noise.

A two-step approach to mitigating the channel Doppler effect was proposed in [5], [18]. The first step is to resample $\tilde{y}(t)$ in the passband with a resampling factor b, which represents our estimate of a, leading to

$$\tilde{z}(t) = \tilde{y}\Big(\frac{t}{1+b}\Big). \tag{44}$$

Converting to baseband, we obtain $z(t)$

$$z(t) = e^{j2\pi \frac{a-b}{1+b} f_c t} \sum_{k \in \mathcal{S}_A} s[k] e^{j2\pi \frac{1+a}{1+b} \frac{k}{T} t} \left[\sum_p A_p e^{-j2\pi f_k \tau_p} g\left(\frac{1+a}{1+b} t - \tau_p \right) \right] + n(t), \tag{45}$$

The second step is to perform fine Doppler shift compensation on $z(t)$ to obtain $z(t)e^{-j2\pi\epsilon t}$, where ϵ is the estimated residual Doppler shift. Performing ZP-OFDM demodulation, the output y_m on the mth subchannel is

$$z_m = \frac{1}{T}\int_0^{T+T_g} z(t)e^{-j2\pi\epsilon t}e^{-j2\pi\frac{m}{T}t}dt. \tag{46}$$

Plugging in the $z(t)$ and carrying out the integration, we simplify y_m to

$$z_m = C\left(\frac{1+b}{1+a}(f_m+\epsilon)\right)\sum_{k\in\mathcal{S}} s[k]\varrho_{m,k} + v_m, \tag{47}$$

where v_m is the additive noise, $C(f)$ is defined in (8), and

$$\varrho_{m,k} = \frac{1+b}{1+a}\cdot\frac{\sin(\pi\beta_{m,k}T)}{\pi\beta_{m,k}T}e^{j\pi\beta_{m,k}T}, \tag{48}$$

$$\beta_{m,k} = (k-m)\frac{1}{T} + \frac{(a-b)f_m - (1+b)\epsilon}{1+a}. \tag{49}$$

Defining the symbol energy as $\sigma_s^2 = E[|s[k]|^2$ and the noise variance as σ_v^2, we find the effective SNR on the mth subcarrier to be:

$$\gamma_m = \frac{|\varrho_{m,m}|^2\sigma_s^2}{\frac{\sigma_v^2}{|C\left(\frac{1+b}{1+a}(f_m+\epsilon)\right)|^2} + \sum_{k\neq m}|\varrho_{m,k}|^2\sigma_s^2}. \tag{50}$$

The first term in the denominator is due to additive noise, while the second term is due to the self-interference aroused by the Doppler scale mismatch. Even when the additive noise diminishes, the effective SNR is bounded by

$$\gamma_m \leq \bar{\gamma}_m := \frac{|\varrho_{m,m}|^2}{\sum_{k\neq m}|\varrho_{m,k}|^2} \tag{51}$$

due to self-interference induced by Doppler scale mismatch.

We now evaluate the SNR uppperbound for two cases:

- Case 1: No Doppler shift compensation by setting $\epsilon = 0$.
- Case 2: Ideal Doppler shift compensation where

$$\epsilon_{\text{opt}} = \frac{a-b}{1+b}f_c, \tag{52}$$

such that

$$\beta_{m,k} = (k-m)\frac{1}{T} + \frac{a-b}{1+a}\cdot\frac{m}{T}. \tag{53}$$

For the first case, the leading term $(k-m)/T$ in $\beta_{m,k}$ is the frequency distance between the kth and the mth subcarriers, while the second term $\frac{a-b}{1+a}f_m$ is the extra frequency shift. For the second case, the leading term $(k-m)/T$ in $\beta_{m,k}$ is the frequency distance between the kth and the mth subcarriers, while the second term $\frac{a-b}{1+a}\cdot\frac{m}{T}$ is the extra frequency shift. Since f_m is much larger than $\frac{m}{T}$, we can see that Doppler shift compensation will improve the performance. Consider an example of $f_c = 27$ kHz and $B/2 = 6$ kHz, we have $f_m \in [21, 33]$ kHz and $\max_m \frac{m}{T} = 6$ kHz. Hence, the accuracy of $(a-b)$ can be relaxed at least by four times to reach similar performance. CFO compensation is one crucial step in the receiver design, which was the key in the success of the receivers in [5], [18].

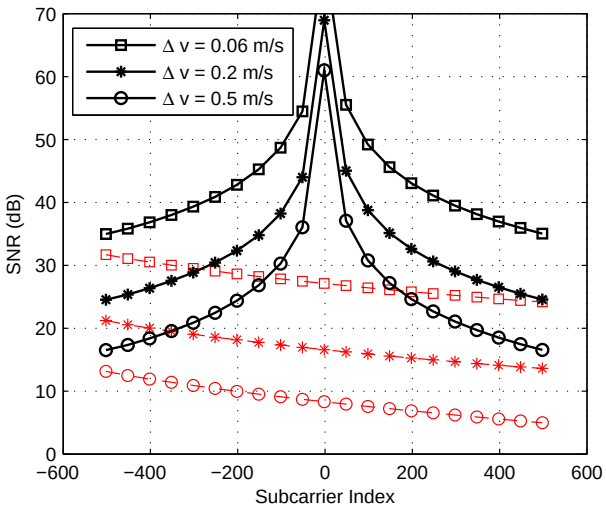

Fig. 5. The SNR upperbound $\bar{\gamma}_m$ for $\epsilon = \epsilon_{\text{opt}}$ (thick, full lines) and $\epsilon = 0$ (thin, dashed lines) as a function of Δv, where $a - b = \Delta v/c$.

We now numerically evaluate the upperbound $\bar{\gamma}_m$ for $\epsilon = 0$ and ϵ_{opt}. We set $f_c = 27$ kHz, $B = 12$ kHz, and $K = 1024$. Fig. 5 shows the bounds for these two cases respectively. Suppose that we want to limit the self noise to be below at least 20 dB below the signal power. In case of $\epsilon = 0$, we need Δv to be less than 0.06 m/s. While in case of ϵ_{opt}, the Δv can be as large as 0.3 m/s.

Fig. 5 provides guidelines on the selection of the Doppler scale spacing of the parallel correlators. For example, assuming that the correlator branch closest to the true speed will yield the maximum metric, then with fine Doppler shift compensation $\epsilon = \epsilon_{\text{opt}}$ we can set the Doppler scale spacing to be 0.4 m/s (where we need Δv to be less than 0.2 m/s) to achieve an SNR upperbound of at least 25 dB. On the other hand, if an SNR upperbound of 15 dB is sufficient, the Doppler scale spacing could be as large as 1.0 m/s.

VI. Implementation and Performance Testing

In Section IV, it was shown that for $K_0 = 512$ OFDM carriers in the preamble, a speed mismatch of up to 1.5 m/s did not degrade the detection performance considerably. On the other hand, the SNR analysis for data reception using $K = 1024$ OFDM subcarriers in Section V indicated that the speed mismatch should not exceed 0.3-0.5 m/s to limit ICI. This suggests a multi-grid approach for the implementation:

1) *Coarse-grid search for detection*. Only a few parallel self-correlators are used to monitor the incoming data. This helps to reduce the receiver complexity.
2) *Fine-grid search for data demodulation*. After a detection is declared, a set of parallel self-correlators with better Doppler scale resolution are used only on the captured preamble. Fine-grid search is centered around the Doppler scale estimate from the coarse-grid search.

Instead of multi-grid search, one may also use an interpolation based approach to improve the estimation accuracy beyond the limit set by the step size. We borrow a technique from [22], which is usually used in spectral peak

location estimation based on a limited amount of DFT samples. After coarse or fine-grid search, let $|X_k|$ denote the amplitude from the branch with the largest correlation output, and $|X_{k-1}|$ and $|X_{k+1}|$ are the amplitudes from the left and right neighbors. Let Δa denote the grid spacing. The formula

$$\delta = \frac{|X_{k+1}| - |X_{k-1}|}{4|X_k| - 2|X_{k-1}| - 2|X_{k+1}|}\Delta a \tag{54}$$

can be used to estimate an offset δ of the Doppler scale deviating from the strongest branch towards the second strongest branch.

A. Simulations for Velocity Estimation

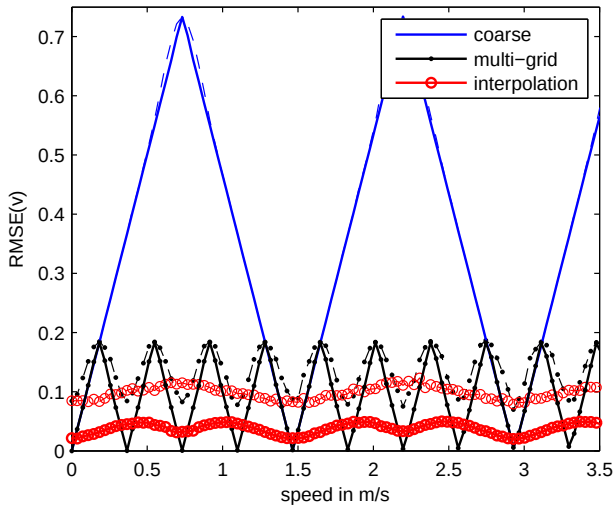

Fig. 6. Average velocity estimation error using varying amounts of correlators and a simple interpolation between the measured points; thin, dashed lines are $\gamma = 0$ dB and thick full lines are $\gamma = 10$ dB.

We use $K_0 = 512$ subcarriers and an oversampling factor of $\lambda = 8$ and set the coarse grid spacing as $\Delta a = \Delta v/c$, where Δv is 1.46 m/s. Fig. 6 depicts the root mean square error of the speed estimates $\hat{v} = c\hat{a}$, at two SNRs of 0 dB and 10 dB. We observe a "saw-tooth" shape for the coarse estimates, and the SNR decrease has little impact on this shape. This suggests that the probability of not finding the closest branch is negligible and the dominating error is the quantization to the coarse grid.

After detection of the coarse-grid search, we use another six self-correlators with spacing of $\Delta v = 0.366$ m/s to search around the estimated Doppler scale from the previous stage. Much improved estimates are obtained, as shown in Fig. 6. The achieved accuracy exceeds the mismatch specification we set earlier of 0.3-0.5 m/s. We can see more degradation of the saw-tooth shape for low SNR. This is reasonable. As the separation in tentative Doppler scales between correlators diminishes, neighboring correlators will have very similar outputs.

Also, Fig. 6 shows the RMSE for velocity estimation with interpolation applied after the coarse grid search with $\Delta_v = 1.46$ m/s. We observe that the interpolation approach is very effective.

B. Results with Experimental Data

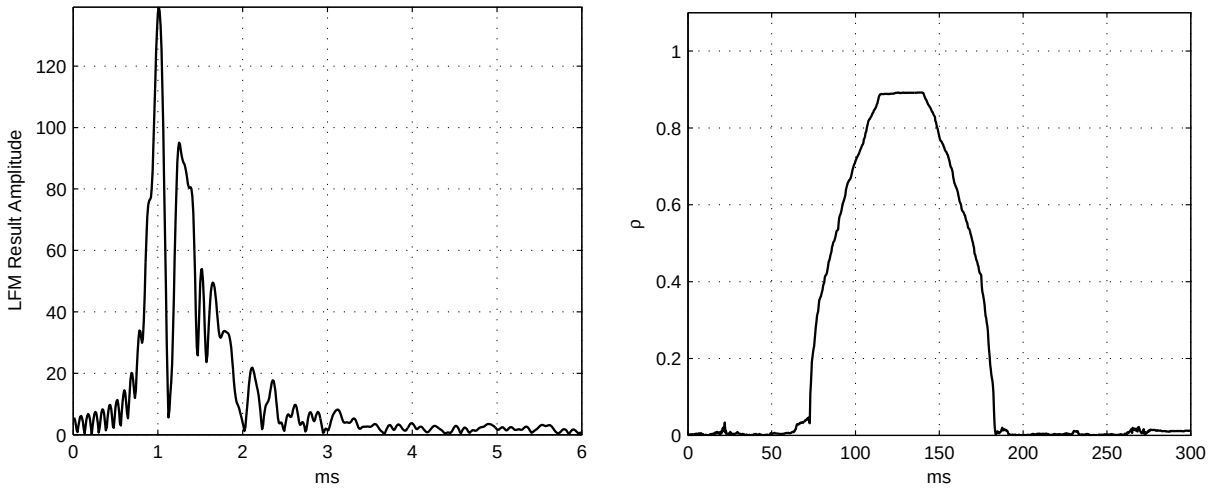

(a) LFM matched filter (b) OFDM self-correlator

Fig. 7. Comparison of the matched filter output for one LFM preamble and the "plateau" output of the proposed synchronization metric.

When the transmitter and the receiver are stationary, Doppler scale estimation is not needed, and only one self-correlation branch is necessary at the receiver. The detection and coarse synchronization algorithms based on one branch have been used in the PC- and DSP-based multicarrier modem prototypes [23], [24].

We now work on the data from an experiment performed at Buzzards Bay, Dec. 15, 2006 with a fast-moving transmitter. The same data set was used previously in [5] to demonstrate the capability of OFDM reception in a dynamic setup. The used packet structure is shown in Fig. 8.

Doppler scale estimation is done in [5] based on the measured time difference between the LFM pre- and postamble. This scheme showed good performance, as after Doppler scale compensation via resampling the data could be decoded with reasonable BER. The drawback is that the whole packet needs to be buffered before data processing.

First we plot a comparison of the timing metrics for a matched filter using the LFM waveform with our proposed scheme in Fig. 7. We observe that the channel energy is fairly constrained within the first 2-3 ms – accordingly the plateau observed at the self-correlator output is almost of length T_{cp}, which in this case is 25.6 ms.

We compare the Doppler scale/relative speed estimation accuracy between the two schemes. In Fig. 9(a) we plot the relative velocity estimates between the sender and receiver; as also an OFDM preamble and postamble were available we include both estimates. Even though these would not both be used for decoding purposes, as real-time operation is the goal, they give intuition about the results, since no ground truth is available. Fig. 9(b) zooms in on the transmissions were the Doppler scale changes dynamically. This was caused by the transmitter passing by closely at the receiver's location around transmission 19. As the Doppler scale is assumed constant during each transmission this will also be the most challenging transmissions to decode.

Fig. 8. The structure of the data packet used in the Buzzards Bay experiment, Dec. 15, 2006.

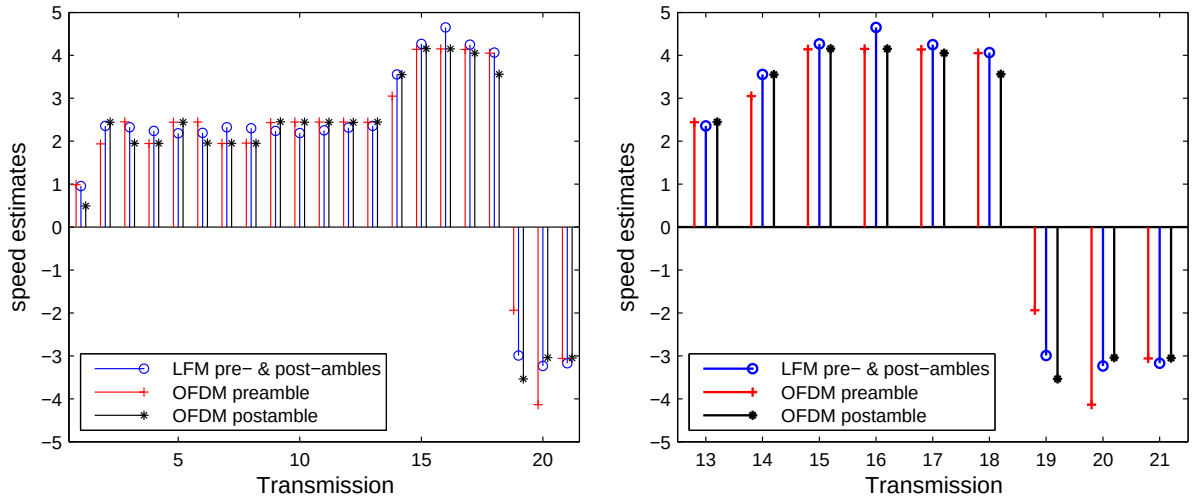

(a) full transmission (b) zoom

Fig. 9. Comparison of velocity estimation techniques; the previous method calculated the time difference between LFM pre- and post-ambles, while the new approach is solely based on either preamble or postamble at one particular time.

Generally the speed estimates are close, when looking at the details (see zoom), it is interesting to consider that the previous method uses the duration of a complete transmission while our new approach is a point estimate. Since the experiment used a large number of OFDM blocks per transmission (32 blocks for the case of 1024 subcarriers), the time-varying nature of the actual Doppler speed is reflected differently in the two approaches. Inspecting the estimates for transmission 14, 16 or 20, the LFM-based result is not the average between the OFDM pre- and postamble point estimates. We observe that this new proposed method differs from the previous method by no more than 1 knot (0.5 m/s) for any transmission.

We next carry out a comparison on the BER performance, where QPSK modulation and a 16-state rate 2/3 convolutional code was used in the data set [5]. Demodulation and decoding were done twice for each packet transmission; once using the Doppler scale estimate obtained from the LFM method and once using the estimate based on *the OFDM preamble only*. Fig. 10 shows that similar uncoded and coded BER results are obtained. The proposed method, however, avoids the need of using the postamble and buffering the whole packet before data demodulation.

The instances where differences in BERs are observed are with transmissions 9 and 18. There are several environmental factors which could have contributed to this anomaly, including ship noise and a more rapid rate of

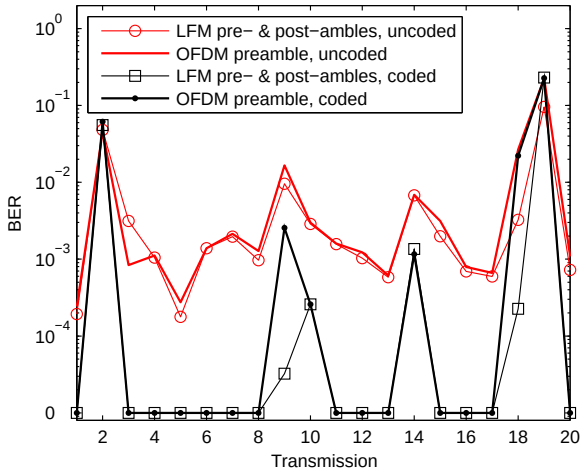

Fig. 10. Comparison of the uncoded and coded bit error rates; decoding after resampling with either the offline speed estimates based on the LFM pre- and post-ambles or based on the new speed estimate for online processing.

change in velocity than experienced by some blocks, which are discussed in [18]. Perhaps since the original method for velocity estimation uses the average compression/dilation over the entire transmission, this new method, which only relies on one preamble sequence, is more susceptible to rapid changes in velocity during a transmission.

Generally the length of the transmitted packets in this experiment was fairly long, e.g, 32 blocks for $K = 1024$ OFDM carriers. This means that due to the dynamic nature of the scenario the Doppler scale has to be estimated more frequently. As the estimation error needs to be below 0.3-0.5 m/s, comparing Fig. 9, if the speed change between preamble and postamble is on this order or above, the Doppler scale estimation error is not limited by the accuracy of the algorithm, but by the frequency of its update.

VII. Conclusion

In this paper we proposed a new method for detection, synchronization, and Doppler scale estimation for underwater communications based on multicarrier waveform. We characterized the receiver operating characteristic and analyzed the impact of Doppler scale mismatch on the system performance. Compared to existing LFM-based approaches, the proposed method works with a constant detection threshold independent of the noise level and is suited to handle the presence of dense multipath channels. More importantly, the proposed approach avoids the need of buffering the whole data packet before data demodulation, which is very appealing for the development of online receivers for multicarrier underwater acoustic communication.

References

[1] M. Chitre, S. H. Ong, and J. Potter, "Performance of coded OFDM in very shallow water channels and snapping shrimp noise," in *Proceedings of MTS/IEEE OCEANS*, vol. 2, 2005, pp. 996–1001.

[2] P. J. Gendron, "Orthogonal frequency division multiplexing with on-off-keying: Noncoherent performance bounds, receiver design and experimental results," *U.S. Navy Journal of Underwater Acoustics*, vol. 56, no. 2, pp. 267–300, Apr. 2006.

[3] M. Stojanovic, "Low complexity OFDM detector for underwater channels," in *Proc. of MTS/IEEE OCEANS conference*, Boston, MA, Sept. 18-21, 2006.

[4] B. Li, S. Zhou, M. Stojanovic, and L. Freitag, "Pilot-tone based ZP-OFDM demodulation for an underwater acoustic channel," in *Proc. of MTS/IEEE OCEANS conference*, Boston, MA, Sept. 18-21, 2006.

[5] B. Li, S. Zhou, M. Stojanovic, L. Freitag, and P. Willett, "Non-uniform Doppler compensation for zero-padded OFDM over fast-varying underwater acoustic channels," in *Proc. of MTS/IEEE OCEANS*, Aberdeen, Scotland, June 2007.

[6] W. Li and J. C. Preisig, "Estimation and equalization of rapidly varying sparse acoustic communication channels," in *OCEANS 2006*. MTS/IEEE, Sept. 2006, pp. 1–6.

[7] Y. R. Zheng, C. Xiao, T. C. Yang, and W.-B. Yang, "Frequency-domain channel estimation and equalization for single carrier underwater acoustic communications," in *Proc. of MTS/IEEE OCEANS conference*, Vancouver, BC, Canada, Sept. 29 - Oct. 4, 2007.

[8] D. B. Kilfoyle, J. C. Preisig, and A. B. Baggeroer, "Spatial modulation experiments in the underwater acoustic channel," *IEEE J. Ocean. Eng.*, vol. 30, no. 2, pp. 406–415, Apr. 2005.

[9] S. Roy, T. M. Duman, V. McDonald, and J. G. Proakis, "High rate communication for underwater acoustic channels using multiple transmitters and space-time coding: Receiver structures and experimental results," *IEEE J. Ocean. Eng.*, Feb. 2007, to be published.

[10] B. Li, S. Zhou, M. Stojanovic, L. Freitag, J. Huang, and P. Willett, "MIMO-OFDM over an underwater acoustic channel," in *Proc. of MTS/IEEE OCEANS conference*, Vancouver, BC, Canada, Sept. 29 - Oct. 4, 2007.

[11] D. B. Kilfoyle and A. B. Baggeroer, "The state of the art in underwater acoustic telemetry," *IEEE J. Ocean. Eng.*, vol. 25, no. 1, pp. 4–27, Jan. 2000.

[12] B. S. Sharif, J. Neasham, O. R. Hinton, and A. E. Adams, "A computationally efficient Doppler compensation system for underwater acoustic communications," *IEEE J. Ocean. Eng.*, vol. 25, no. 1, pp. 52–61, Jan. 2000.

[13] T. M. Schmidl and D. C. Cox, "Robust frequency and timing synchronization for OFDM," *IEEE Trans. Commun.*, vol. 45, no. 12, pp. 1613–1621, Dec. 1997.

[14] H. Minn, V. Bhargava, and K. Letaief, "A robust timing and frequency synchronization for OFDM systems," *IEEE Trans. Wireless Commun.*, vol. 2, no. 4, pp. 822–839, July 2003.

[15] R. D. J. van Nee, G. A. Awater, M. Morikura, H. Takanashi, M. A. Webster, and K. W. Halford, "New high-rate wireless LAN standards," *IEEE Communications Magazine*, vol. 37, no. 12, pp. 82–88, Dec. 1999.

[16] E. G. Larsson, G. Liu, J. Li, and G. B. Giannakis, "Joint symbol timing and channel estimation for OFDM based WLANs," *IEEE Commun. Lett.*, vol. 5, no. 8, pp. 325–327, Aug. 2001.

[17] C. R. Berger, S. Zhou, Z. Tian, and P. Willett, "Performance analysis on an MAP fine timing algorithm in UWB multiband OFDM," *IEEE Trans. Commun.*, 2008 (to appear); downloadable at http://www.engr.uconn.edu/˜shengli/BZTW08.pdf.

[18] B. Li, S. Zhou, M. Stojanovic, L. Freitag, and P. Willett, "Multicarrier communication over underwater acoustic channels with nonuniform Doppler shifts," *IEEE J. Ocean. Eng.*, 2008 (to appear); downloadable at http://www.engr.uconn.edu/˜shengli/LZSF08joe.pdf.

[19] J. H. Conway, R. H. Hardin, and N. J. A. Sloane, "Packing lines, planes, etc.: Packings in Grassmannian space," *Experimental Math.*, vol. 5, no. 2, pp. 139–159, 1996.

[20] S. Zhou, Z. Wang, and G. B. Giannakis, "Quantifying the power-loss when transmit-beamforming relies on finite rate feedback," *IEEE Trans. Wireless Commun.*, vol. 4, no. 4, pp. 1948–1957, July 2005.

[21] K. Mukkavilli, A. Sabharwal, E. Erkip, and B. Aazhang, "On beamforming with finite rate feedback in multiple-antenna systems," *IEEE Trans. Inform. Theory*, vol. 49, no. 10, pp. 2562–2579, Oct. 2003.

[22] E. Jacobsen and P. Kootsookos, "Fast, accurate frequency estimators [DSP Tips & Tricks]," *IEEE Signal Processing Magazine*, vol. 24, no. 3, pp. 123–125, May 2007.

[23] S. Mason, R. Anstett, N. Anicette, and S. Zhou, "A broadband underwater acoustic modem implementation using coherent OFDM," in *Proc. of National Conference for Undergraduate Research (NCUR)*, San Rafael, California, Apr. 2007.

[24] H. Yan, S. Zhou, Z. Shi, and B. Li, "A DSP implementation of OFDM acoustic modem," in *Proc. of the ACM International Workshop on UnderWater Networks (WUWNet)*, Montréal, Québec, Canada, Sept. 2007.